Correlation of Heat Loss with Quenching Distance During Transient Flame-Wall Interaction

Feichi Zhang[a,b,*], Thorsten Zirwes[b,c,d], Thomas Häber[e], Henning Bockhorn[b], Dimosthenis Trimis[b], Rainer Suntz[e], Dieter Stapf[a]

[a]*Institute for Technical Chemistry, Karlsruhe Institute of Technology, Hermann-von-Helmholtz-Platz 1, 76344, Eggenstein-Leopoldshafen, Germany*
[b]*Engler-Bunte-Institute, Division of Combustion Technology, Karlsruhe Institute of Technology, Engler-Bunte-Ring 1, 76131 Karlsruhe, Germany*
[c]*Steinbuch Centre for Computing (SCC), Karlsruhe Institute of Technology, 76344, Eggenstein-Leopoldshafen, Germany*
[d]*Department of Mechanical Engineering, Stanford University, Stanford CA 94305, USA*
[e]*Institute for Chemical Technology and Polymer Chemistry, Karlsruhe Institute of Technology, Engesserstr. 20, 76131, Karlsruhe, Germany*

Abstract

Detailed numerical simulations of stoichiometric premixed methane/air flames have been conducted for a side-wall-quenching (SWQ) setup, in order to study the effect of transient motion of the flame on flame-wall interaction (FWI). A W-shaped plane-jet (2D) flame is considered, which is bounded in its lateral direction by walls. The left wall oscillates in its normal direction with pre-defined frequencies f and stroke lengths L (distance between the minimum and maximum wall locations), exciting the entire flow and resulting in an unsteady motion of the flame at the left and right wall. While the instantaneous flame contours near the moving and the stationary wall differ, the instantaneous quenching distance d_q and wall heat flux $\dot{q}_w$ at the walls yield a quasi-linear correlation in the case of low f and L. However, hysteresis loops with a weakened correlation for $\dot{q}_w$ vs. d_q have been detected for large f and L, which leads to a considerably increased time-averaged d_q and decreased time-mean $\dot{q}_w$ compared with results obtained from the steady-state solution. The reason is attributed to the delayed response of the flame to the rapidly varying temperature and flow fields caused by the transient motion of the flame with respect to the wall. In this case, the flame requires a relaxation time to perceive the heat flux to the wall and to adjust its dynamics. The results indicate an essential impact of the unsteady flow nature on FWI, which has to be considered for turbulent combustion modeling. A quasi-linear correlation between the volumetric heat loss rate caused by the wall and the time-mean d_q has been proposed for a first-order estimate of the effect of FWI, which could be implemented into the energy balance as sink term for modeling turbulent flame propagation under the influence of a cold wall.

Keywords: Flame-turbulence-wall interaction; Side wall quenching; Quenching distance; Wall heat flux; Detailed numerical simulation.

*Feichi Zhang
Email address: Feichi.Zhang@kit.edu (Feichi Zhang)

1. Introduction

Flame-wall interaction (FWI) constitutes a common issue in engineering combustion applications with high power density, such as in internal combustion engines or gas turbines. There, the flame propagates against a cold wall and is extinguished in a thin layer close to the wall due to extreme heat loss. The effect of FWI contributes significantly to phenomena such as flame stabilization, burning efficiency and lifetime of the combustor. Due to its importance, FWI has been studied extensively in the last decades with measurements and numerical simulations [1–20]. Dreizler and Böhm [1] and Kosaka et al. [8] performed comprehensive laser diagnostics with detailed measurements of near-wall flow and temperature fields. The same test rig has then been studied via large eddy simulations (LES) and direct numerical simulations (DNS) in 2D/3D setups and with different reaction-diffusion models in [3, 4]. Häber and Suntz [5] and Strassacker et al. [6] conducted measurements and numerical simulations on stationary side-wall quenching (SWQ) of premixed methane/air flames at different equivalence ratios and have shown that the quenching distance is only weakly dependent on the wall material and heterogeneous reactions. Gruber et al. [14] studied a turbulent V-shaped hydrogen/air premixed flame anchored in a fully developed channel flow by means of 3D DNS. They found a regime transition from the thin flamelet to the thickened flame regime, when the flame approaches a cold wall. Mejia et al. [7] studied the influence of wall temperatures on the flame response to acoustic perturbations, where the flame instability can be controlled or suppressed by changing solely the temperature of the burner rim. The DNS by Poinsot et al. [9] indicates that the quenching distances and the maximum heat fluxes in a turbulent flow remain of the same order as for laminar flames and the wall acts as a sink for the flame surface density. Popp and Baum [15] presented a numerical study of FWI for a stoichiometric methane/air flame. Using an approach with a single step chemical reaction, the heat flux through the wall could not be predicted accurate enough. Mann et al. [12] and Luo et al. [13] performed experimental and numerical studies of 1D strained laminar premixed flames impinging on a wall (head-on-quenching – HOQ), where an increase of strain rate leads to a reduced quenching distance and an increase in the wall heat flux. Zhang et al. [16] studied flame dynamics in terms of flame stretch and flame speed using 2D DNS for a stationary SWQ setup with methane/air flames, where the Markstein number reverses its sign while the flame approaches the wall. Zhao et al. [11] performed 3D DNS of premixed turbulent combustion for a HOQ flame, dividing the FWI zone into an "influence zone", where the flame temperature and scalar gradients start to decrease, and a "quenching zone", where chemical reactions become negligible. Wang et al. [19, 20] have performed 3D DNS for turbulent FWI using detailed reaction kinetics, where the quenching distance was shown to be negatively correlated with wall heat flux in both premixed and non-premixed flames. A novel back-on quenching mode for FWI was introduced in [19], which leads to the lowest heat release rate at the wall. In an a priori analysis made for DNS of turbulent SWQ in a channel [21], the PDF (probability density function) closure models have shown a high accuracy in the core flow. However, only the quadrature-based moment methods (QBMM) was able to predict the flame structures in the near-wall region.

Despite the progress achieved in the previous works, detailed knowledge with regard to an in-depth understanding and prediction of the FWI behavior is missing. As the flame extinguishes at a wall distance of the order of 0.1 mm, studying FWI still remains a challenging task. It is even further complicated by the transient nature of the turbulent flow, which leads to a triple interaction between the flame, turbulence and wall. Previous experimental studies of FWI have been performed mostly for steady-state conditions, disregarding the time history effect caused by the unsteady flow. The numerical simulations of turbulent FWI have focused mainly on the statistical correlations between the chemical scalars in the FWI zone or comparison with measured data for model validation. Mostly simplified calculations for the reaction rate and transport coefficients (e.g. unity Lewis number) were applied in these works to reduce computational cost. Until now, there are no reliable models to account for the effect of FWI, and a knowledge gap exists between the stationary and transient behavior for understanding the FWI process, which constitutes the objective of this work.

In order to reveal systematically the influence of unsteady relative motion between the flame and wall on FWI, numerical simulations using detailed calculations of chemical reaction rates and transport coefficients have been performed for a generic 2D SWQ configuration with well-defined boundary conditions. The unsteady flame motion has been generated by a transversely oscillating side wall with prescribed frequencies and amplitudes, which excites the flame and leads to unsteady FWI at both walls. A special focus of this work is to assess quantitatively the resulting quenching distance and wall heat flux, as well as their correlations with time and length scale of the relative motion be-

tween the flame and the wall.

In the following, the numerical setups used for the simulations are presented in Sec.2. The simulation results are discussed in detail in Sec.3 with respect to flame's local and global dynamics, respectively. The work is summarized in Sec.4.

2. Numerical setups

2.1. Computational domain and boundary conditions

Detailed numerical simulations, which fully resolve the flame front while applying detailed reaction kinetics and transport properties, have been conducted for a 2D SWQ setup operated with stoichiometric premixed methane/air flames at atmospheric condition. A rectangular shaped domain with a height of 32 mm and width of 16 mm is used, which encloses a W–shaped flame bounded by sidewalls in the lateral direction, as shown in Fig.1. The fresh gas and wall temperatures are set to $T_w = 293$ K. The flame is stabilized by a gas flow with multiple parabolic velocity profiles at the inlet, which have a minimum velocity of 0 m/s at 1/4 and 3/4 of the domain width. The maximum velocity of the parabolic profile is 1.6 m/s, which leads to a bulk flow velocity of $u_{\text{bulk}} \approx 3S_l^0$, with the unstretched laminar burning velocity $S_l^0 = 0.32$ m/s obtained from calculations of a 1D unstretched laminar premixed flame. The burnt gas leaves the domain at the outlet, where the gradients of all flow variables are set to zero. The front and back sides of the domain have been set as symmetry planes.

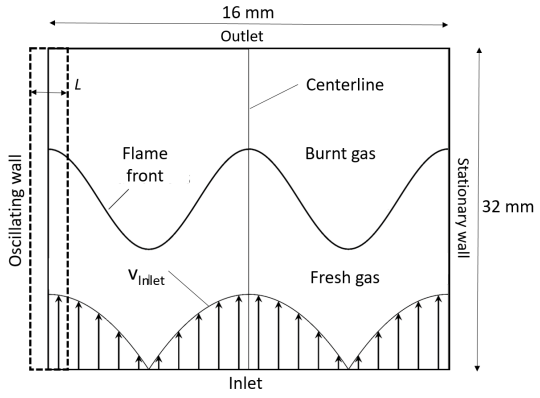

Figure 1: Schematic setup and boundary conditions used for detailed numerical simulations of unsteady side-wall quenching.

The unsteady motion of the flame has been accomplished by an oscillatory motion of the left wall in its normal direction, whereas the right wall remains stationary. The position of the left wall changes in a sinusoidal way with a pre-defined frequency f and stroke length L (distance between the min/max wall locations). In this way, the entire flame is excited by the oscillatory motion of the left wall, which leads to two scenarios with transient, relative motion between the flame and wall: (1) the left flame is disturbed directly by the moving wall; (2) the right flame is excited by the moving wall due to compression/expansion of the flow domain, which interacts with the stationary right wall.

The relative motion between the flame and wall reflects the situation when a turbulent, unsteady flame propagates against a stationary wall in a combustion chamber. The frequency f and the stroke range L have been varied in the range of $f = [50, 100, 200]$ Hz and $L = [1, 2]$ mm, which are selected to sustain the laminar flow nature. With further increased f and/or L, the flow tends to attain the turbulent flow, which results in strongly curved flames. As only a 2D grid is used in this work, the onset of turbulent flow cannot be captured. In reality, the interaction of an instationary wall with a flame can be found in internal combustion engines with a moving piston; moreover, large pressure fluctuations during constant-volume combustion, e.g. in gas turbines during high-load operation, may lead to vibration of the chamber wall, which interacts with the flame.

2.2. Solution setups

An in-house developed solver in OpenFOAM has been used, where OpenFOAM for numerical solution of the balance equations is coupled with the chemical library Cantera [22, 23] to account for detailed calculations of chemical reaction rates and transport coefficients. The governing equations are solved in their compressible formulations, employing a fully implicit scheme of second order (backward) for the time integration and a fourth order interpolation scheme for discretization of the convective term. All diffusive terms are discretized with an unbounded scheme of fourth order accuracy, too. The pressure-implicit split-operator (PISO) algorithm has been used for pressure correction. A detailed description along with validations of the numerical solver can be found in [22–25]. The chemical reactions for methane/air combustion are described by the GRI-3.0 mechanism [26] and molecular diffusion is considered by the mixture-averaged transport model.

An equidistant grid length with $\Delta = 40$ μm is used, which resolves the unstretched laminar flame thickness δ_l^0 with more than 10 cells. Further simulations performed on a twice-refined grid with $\Delta = 20$ μm have shown almost the same results for the resolved quenching distance (see Sec.3.3 and Fig.9), which validates the grid resolution used in this work. A dynamic mesh technique has been used to account for the oscillatory mov-

ing wall, where the mesh topology remains unchanged during compression or expansion of the domain. As the oscillation amplitude of the left wall with 1 or 2 mm is small compared with the width of the domain (16 mm), the grid is stretched only slightly by the moving wall. The simulations have been run with a time step of 0.5 μs, allowing a maximum convective CFL (Courant–Friedrichs–Lewy) number of 0.2.

3. Results

3.1. Flame stabilization during steady-state FWI

Figure 2 provides an overview of the simulation results for the steady-state case with both lateral side walls set as stationary. The figure presents the contours of the streamwise velocity u (left) and temperature T (right). Streamlines are depicted to illustrate the flow directions and the solid line on the right indicates the flame surface identified by the isotherm $T = 1452$ K, corresponding to the temperature at the location with the largest gradient of heat release rate from 1D unstrained flame calculations [8]. As the flame is symmetric to the centerline axis for the steady-state case, only the left half of the flame is presented. Overall, the flame is stabilized close to the low velocity region given by the parabolic velocity profile at the inlet ($u = 0$ at $x = 4$ mm). In the FWI zone, the flame is stabilized based on a local balance between the flow velocity and the flame propagation speed, which decrease to 0 while approaching the wall. The flame is extinguished while approaching the side-wall, which can be detected from contours of T in Fig.2 , where T decreases to T_W. The flow is accelerated by passing through the flame front in its normal direction, leading to bending of the streamlines at the flame surface. As a consequence, the thicknesses of the temperature and velocity boundary layers increase in the streamwise direction at the point of FWI, which is identified by the location of the smallest distance between the flame surface and wall.

A zoomed view of u and T into the FWI zone is shown in Fig.3, where iso-contours of the heat release rate are used to indicate the reaction zone. For common freely propagating flames without influence of the wall, flame stabilization is achieved by a competition between the flame's displacement speed and flow velocity. For the SWQ case, the flame is "pushed away" from the wall due to acceleration of the flow along the flame-normal direction, as shown by the deflected streamlines at the flame tip in Fig.3. At the same time, the flame propagates towards the fresh gas in the vicinity of the wall and is stabilized at the position where the local flame

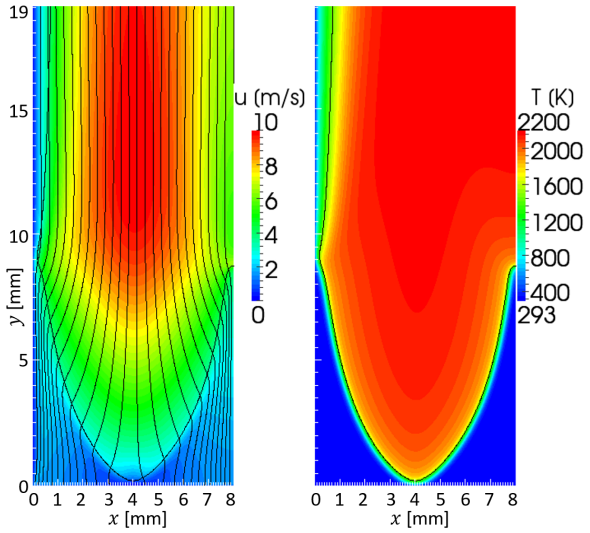

Figure 2: Contours of streamwise velocity (left) and temperature (right) calculated from simulation of a stationary CH_4/air SWQ flame. Streamlines and flame surface are indicated by solid black lines.

speed and near-wall flow velocity are in balance. As the flow in the near-wall region is intrinsically laminar due to the non-slip condition, the flame is stabilized at a relatively low propagation speed, which is of the order of S_l^0, and the quenching distance is of the order of the laminar flame (thermal) thickness δ_l^0 [5]. The flame is negatively curved and the flow velocity decreases towards the FWI zone, which results in addition to the heat loss in a negative flame stretch and a decrease of the local flame speed at the flame tip [16].

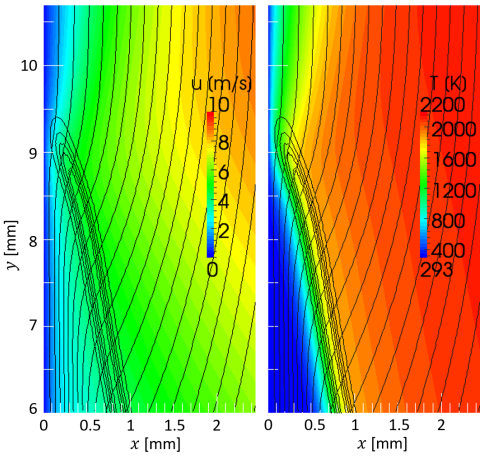

Figure 3: Detailed view of the FWI zone with contours of streamwise velocity on the left and temperature on the right. Streamlines and heat release iso-lines are indicated by solid black lines.

3.2. *Effect of unsteady FWI*

Figure 4 illustrates contours of calculated heat release rate $\dot{q}$ with an oscillatory left wall at $L = 2$ mm for a time instant corresponding to the rightmost position of the wall. The oscillatory motion of the wall leads to periodical compression and expansion of the domain, which results in oscillations of the flow velocity in the whole domain. Accordingly, the W-shaped flame is brought to an excited state, which interacts with the left moving wall and the right stationary wall. Under highly unsteady conditions with large f, the flame becomes wrinkled or curved at its tip on the left, as shown in Fig.4 for 200 Hz. The flow exhibits a transition to the turbulent regime with further increased f and L, so that the 2D assumption made for the current simulation is violated. Therefore, only the cases with $f \leq 200$ Hz and $L \leq 2$ mm are considered in this work.

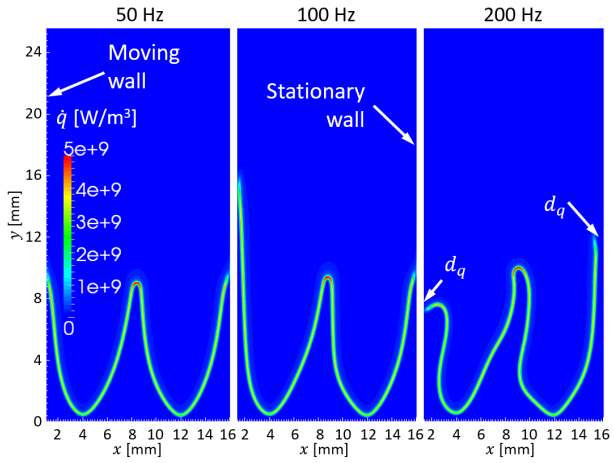

Figure 4: Instantaneous contours of heat release rate calculated from simulation of unsteady FWI using an oscillatory moving left wall.

In the current work, the quenching distance d_q and the wall heat flux $\dot{q}_w$ are evaluated at the location of the smallest distance between the flame and the wall. The flame surface is identified by the isotherm $T = 1452$ K, corresponding to the temperature at the location with the largest gradient of heat release rate from 1D unstrained flame calculations. The relative motion between the flame and the wall results in time fluctuations of the flow velocities and temperature within the FWI zone, which lead to periodic variations of d_q and $\dot{q}_w$. d_q represents a measure for flame dynamics attributed to the non-uniform flow and the flame propagation itself. $\dot{q}_w$ points in the wall-normal direction and is calculated directly at the wall by $\dot{q}_w = \kappa|\nabla T|_w$ at the location of d_q, with κ being the thermal conductivity of the gas mixture.

Figure 5 shows temporal evolution of d_q (top) and $\dot{q}_w$ (bottom) evaluated at the right stationary wall and for the cases with $L = 1$ mm (left) and $L = 2$ mm (right). $\dot{q}_w$ and d_q are negatively correlated (compare the maximum and minimum values of d_q and $\dot{q}_w$ in Fig.5). This is attributed to the fact that a decrease of d_q results in a higher gradient of temperature on the wall and, hence, an increase of $\dot{q}_w$ ($\dot{q}_w \propto |\nabla T|_w$). d_q is increased and $\dot{q}_w$ is decreased under unsteady conditions compared with the steady-state solutions, given by the horizontal solid lines in Fig.5. As an explanation, the flame can propagate freely away from the wall, whereas its motion is limited while approaching the wall. Moreover, d_q and $\dot{q}_w$ yield a phase shift with increased f and L, as indicated in Fig.5 on the right by the time instants t_2 with the maximum of d_q and t_3 with the minimum of $\dot{q}_w$. This denotes a delayed response of $\dot{q}_w$ to d_q due to the unsteadily changing flow and temperature fields. Although not shown here, qualitatively similar results regarding the behavior of d_q and $\dot{q}_w$ in the FWI zone have been obtained for the left moving wall.

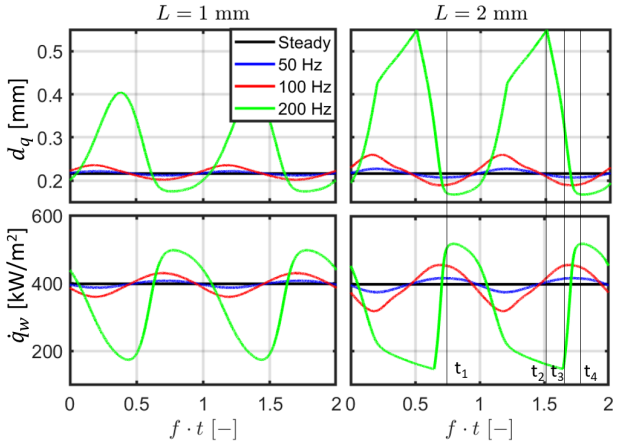

Figure 5: Time development of the quenching distance (top) and the wall heat flux (bottom) at the right stationary wall: on the left for the case with $L = 1$ mm and on the right for the case with $L = 2$ mm.

In Fig.6, $\dot{q}_w$ and d_q from Fig.5 calculated for the right stationary wall are plotted in a phase diagram, at the top for $L = 1$ mm and at the bottom for $L = 2$ mm. The arrows denote the time evolution of the oscillation process, which starts from the minimum value of d_q and turns in clockwise direction. The solid circles indicate the stationary solution. As shown in Fig.5, d_q and $\dot{q}_w$ are generally negatively correlated. For $f = 50$ and 100 Hz, the time development of d_q and $\dot{q}_w$ shown in Fig.5 yields only small phase shifts, indicating that the flame is able to follow promptly the unsteady fluctuations of flow and temperature. Hence, a quasi-linear correlation

is found for d_q and $\dot{q}_w$ in Fig.6 for this case. In case of large f and L, however, $\dot{q}_w$ is timely delayed with respect to the rapid change of d_q, which results in a noticeable phase shift between the time development of d_q and $\dot{q}_w$, as shown in Fig.5 on the right by the curves for f = 200 Hz. This leads to formation of a hysteresis loop with weakened correlation between d_q and $\dot{q}_w$, as shown in Fig.6 at the bottom. The correlation between d_q and $\dot{q}_w$ is stronger in the range of small d_q compared with that of large d_q, because the flame has limited freedom to move close to the wall and, hence, the fluctuations of the flow variables are attenuated in case of small d_q. Although not shown here, qualitatively similar results can also be evaluated for the FWI on the left moving wall.

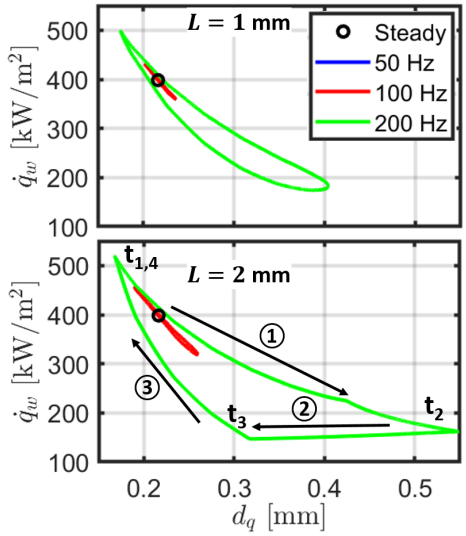

Figure 6: Correlations of instantaneous wall heat flux $\dot{q}_w$ with quenching distance d_q during unsteady FWI at the right, stationary wall.

The formation of the hysteresis loop caused by unsteady FWI is further elucidated in Fig.7, where t_1 to t_4 and ① to ③ correspond to the time instants or scenarios indicated in Fig.5 and Fig.6 by the arrows. The overall process can be divided into 3 stages:

① t_1 to t_2 (d_q ↑, $\dot{q}_w$ ↓): the flame and the wall move away from each other, which leads to a weakened heat loss or decreased $\dot{q}_w$.

② t_2 to t_3 (d_q ↓, $\dot{q}_w \approx const.$): after the maximum flame-wall distance is reached at t_2, the flame and the wall move relatively towards each other; the heat flux remains, however, almost constant.

③ t_3 or t_4 (d_q ↓, $\dot{q}_w$ ↑): with further decreased d_q, $\dot{q}_w$ increases drastically, until the smallest wall distance is reached. The initial state is recovered at this point and the oscillation process starts over again.

It is clear from the above observation that the hysteresis loop shown in Fig.6 is caused during turnaround of the flame at the maximum distance to the wall, where the delayed response of $\dot{q}_w$ to d_q results in a disproportionate correlation between these variables. The turning point at $d_{q,max}$ corresponds to the time instant when the relative motion between the flame and the wall changes its states from moving apart (d_q ↑) to moving towards each other (d_q ↓). It recovers additionally the largest temporal change of the absolute velocity of the flame with respect to the wall, which reverses its sign from positive to negative. The behavior can be explained by a retroactive or inertia effect, where the flame retains its previous state for a short while, or it requires a relaxation time to be updated according to the quickly changing environment. In other words, when the flame moves suddenly with a high speed towards the wall, it yields a certain time delay to follow the moving wall and to sense the heat flux from the cold wall.

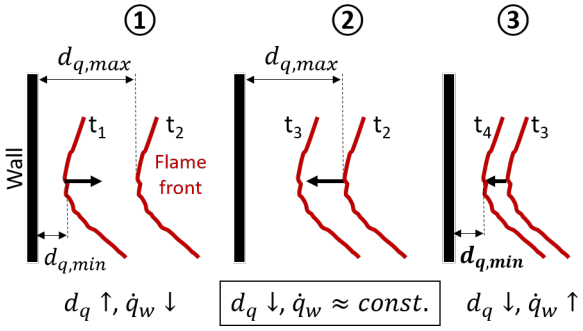

Figure 7: Different scenarios during highly unsteady FWI.

In [27], SWQ using forced inflow at different frequencies has been studied experimentally for a premixed propane/air flame, where the flame shape becomes strongly curved at increased f and the flame surface yields a wider range of shapes throughout the forcing period. The same behavior is obtained in this work, as shown in Fig.4. However, it has been shown in [27] that increasing f has a non-monotonic effect on d_q. Similar result has been reported in [17] by detailed numerical simulations of a forced premixed methane/air flame in SWQ setup, where d_q has been shown to be insensitive to the unsteady inflow. Although the non-dimensional frequency or the Strouhal number St (defined as $St = fL_f/u_{bulk}$ with the flame length L_f) applied in this work, with St = 0.6, 1.2 and 2.4 for f = 50, 100 and 200 Hz, is comparable with that used in [27], d_q has been found to be considerably increased with St or f in the current work. The reason is attributed to the fact that the forced inflows used in [17, 27] essen-

tially led to a longitudinal motion of the flame sweeping along the wall. In contrary, the current setup with an oscillatory wall generates an unsteady relative motion of the flame specifically in the wall-normal direction. Furthermore, the 2D DNS of forced SWQ flames in [28] have shown a strong increase of d_q up to $St = 1$, which is caused by flame motions in the wall-normal direction. However, d_q decreases to the laminar steady-state solution and remains almost constant at $St = 8.3$ in [28]. In this case, the flame was not able to respond to the high-frequency fluctuations of the inflow [29–31].

3.3. Correlation between time-averaged wall heat flux and quenching distance

Figure 8 depicts the time-averaged, normalized quenching distance $\bar{d}_q/\delta_l^0$ (left) and heat flux $\bar{\dot{q}}_w$ (right) for the moving and stationary wall, where the horizontal solid lines denote results from the steady-state solution. In accordance with the time development of d_q and $\dot{q}_w$ shown in Fig.5, $\bar{d}_q$ increases and $\bar{\dot{q}}_w$ decreases with f and L. In addition, $\bar{d}_q$ and $\bar{\dot{q}}_w$ yield a strong negative correlation for both cases. For the most unsteady condition studied in this work with $f = 200$ Hz, the increment of $\bar{d}_q$ is as large as approx. 70% compared with d_q from the steady-state solution, which reveals the significant impact of the transient flame motion on FWI. The flame becomes unstable and is strongly curved under the condition of $L = 2$ mm and $f = 200$ Hz, which leads to multiple FWI zones at the left wall (see Fig.4 on the right). Therefore, defining d_q by the smallest distance between flame surface and wall becomes ambiguous and no results are shown in Fig.8 for this case.

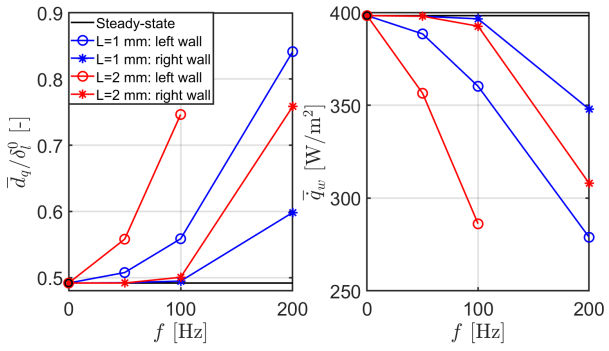

Figure 8: Calculated time-averaged quenching distance (left) and wall heat flux (right) from simulations of unsteady flame-wall interaction.

In Fig.9 at the top, data pairs of $\bar{\dot{q}}_w$ and $\bar{d}_q/\delta_l^0$ given in Fig.8 are plotted, where the solid line represents the linear fit of $\bar{\dot{q}}_w$ vs. $\bar{d}_q/\delta_l^0$. The result reveals a strong correlation between $\bar{\dot{q}}_w$ and $\bar{d}_q$, which is almost not affected by the unsteady nature of the FWI. The lower part of Fig.9 depicts the volume-specific heat flux to the wall $\bar{\dot{\omega}}_w = \bar{\dot{q}}_w/\bar{d}_q$ against $\bar{d}_q/\delta_l^0$, which yields an even stronger correlation compared with that of $\bar{\dot{q}}_w$ vs. $\bar{d}_q/\delta_l^0$ shown in Fig.9 at the top. As shown in Fig.6, the instantaneous quenching distance and wall heat flux yield a non-linear correlation under highly unsteady conditions. However, given the limited number of data points, the correlation between the time-average values $\bar{\dot{q}}_w$ and $\bar{d}_q/\delta_l^0$ can be approximated with reasonable accuracy by a linear model, but is limited to the given range of data.

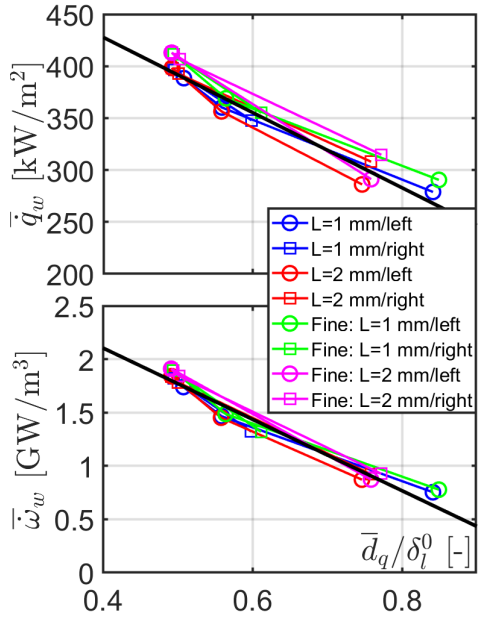

Figure 9: Quasi-linear correlations for the time-mean wall heat flux (top) and volumetric heat loss rate (bottom) with the normalized time mean quenching distance during unsteady FWI.

In order to validate the grid resolution used in this work, the green and magenta curves shown in Fig.9 are calculated from simulations applying a twice refined grid for the cases with $f = 0$ Hz (steady-state), 100 Hz and 200 Hz at $L = 1$ and 2 mm. In the stationary case, both the reference grid used in the current work with $\Delta = 40$ μm and the fine grid with $\Delta = 20$ μm yield an almost identical d_q; in addition, $\dot{q}_w$ obtained from the fine grid is approx. 3% higher in magnitude compared with $\dot{q}_w$ calculated from the reference grid. For the other cases with oscillating walls, the results derived from the reference and fine grids show quantitatively good agreement too. As shown in the lower part of Fig.9, the data pairs of $\bar{\dot{\omega}}_w$ and $\bar{d}_q/\delta_l^0$ calculated from the fine grid lie closely on the fitted line obtained from the reference grid, which validates the grid resolution used in this work.

In summary, it can be stated that the transient motion of the flame relative to the wall leads to a considerably increased $\bar{d}_q$ and decreased $\bar{\dot{q}}_w$. The effect becomes stronger with increased length (in terms of L) and decreased time scales (in terms of $1/f$) of the unsteady motion. The ratio of $\bar{\dot{q}}_w$ and $\bar{d}_q$, which represents a measure for the volumetric heat loss sensed by the flame, decreases almost linearly with $\bar{d}_q$. This correlation is not affected by the unsteady nature, so that the proposed best-fit curve (solid line in Fig.9) may be used to model the effect of heat loss caused by FWI during turbulent combustion. In this case, $\overline{\dot{\omega}}_w$ as a function of $\bar{d}_q$ can be implemented as a sink term in the energy balance, which is effective only in the near-wall or FWI zone.

The overall behavior for the triple flow-flame-wall interaction is illustrated in Fig.10. The flame is stabilized via a competition between the flow and own propagation, which determines the distance between the wall and the flame d_q. On the other hand, the flame perceives a heat flux $\dot{q}_w$ to the wall, which alters the flame's internal structure and its dynamics. At the same time, the flow is slowed down near the wall due to the non-slip condition and is accelerated at the flame front via thermal expansion, which in turn influences the flame through stretch. The heating of the wall by the flame is neglected here. All these processes are connected achieving a balance under steady-state condition. In an unsteady flow, whih is generated in this work by means of an oscillating wall, the flame is subjected to temporal fluctuating heat loss and stretch, so that the flame requires a relaxation time to update its dynamics to the current flow and temperature conditions. As shown in Fig.10 on the right, a flow disturbance with f and L results in an onset of flame motion; the flame speed S_l decreases while approaching the wall due to heat loss, so that the flame is forced to move away from the wall; S_l increases again while the effect of heat loss is reduced and the flame turns to move back towards the wall. The behavior can be described with an enclosed cycle of flame motion towards and away from the wall, which leads to the hysteresis loop for d_q and $\dot{q}_w$ in case of highly unsteady flow, as shown in Fig.6. A balance between the reaction-diffusion processes cannot be achieved due to the delayed responses of the flame to the fluctuating flow velocity and heat flux, which leads to non-zero transient terms in the governing equations.

4. Conclusions

Detail numerical simulations have been conducted to study unsteady flame-wall interaction (FWI). A generic setup using an oscillatory moving wall at prescribed

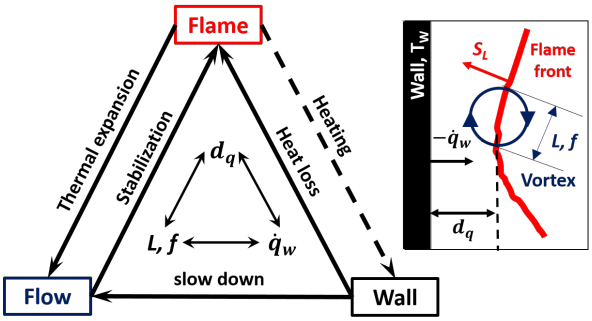

Figure 10: Illustration of fundamental processes during the triple flame-flow-wall interactions.

frequencies f and stroke lengths L has been used to generate unsteady FWI scenarios at the walls. The main findings are listed below:

- the quenching distance d_q is increased and the wall heat flux $\dot{q}_w$ is decreased in an unsteady flow
- $\dot{q}_w$ and d_q are correlated strongly for low f and L
- the time development of d_q and $\dot{q}_w$ yield phase shifts at large f and L, resulting in a hysteresis loop with weakened correlation between $\dot{q}_w$ and d_q
- the time mean values of $\dot{q}_w$ and d_q reveal a quasi-linear, negative correlation, which is not affected by the unsteady flow conditions

The unsteady motion of the flame has a significant impact on the FWI, which has to be accounted for in addition to the general thermo-physical parameters of the mixture. The correlation obtained in this work with the volumetric wall heat loss as a function of d_q can be used for modeling the influence of FWI during turbulent combustion. It should be noted that the effect of the transversal motion of the flame in wall-normal direction is studied in this work, whereas the flame motion in the longitudinal direction (parallel to the wall) plays a subordinate role. The current work is focused on methane/air flames at stoichiometric conditions and a fixed wall temperature of 293 K. Future work with extended operating parameters will demonstrate the validity of this approach.

Acknowledgments

The authors gratefully acknowledge the financial support by the Helmholtz Association of German Research Centers (HGF), within the research field MTET (38.05.01) and the German Research Foundation (DFG), grant number 237267381 – TRR 150. The work was supported by the PRIME programme of the German Academic Exchange Service (DAAD) with funds

from the German Federal Ministry of Education and Research (BMBF). This work utilized computing resources provided by the High Performance Computing Center Stuttgart and the Steinbuch Centre for Computing (SCC) at the Karlsruhe Institute of Technology.

References

[1] A. Dreizler, B. Böhm, Advanced laser diagnostics for an improved understanding of premixed flame-wall interactions, Proc. Comubst. Inst. 35 (1) (2015) 37–64.

[2] C. Jainski, M. Rißmann, B. Böhm, J. Janicka, A. Dreizler, Sidewall quenching of atmospheric laminar premixed flames studied by laser-based diagnostics, Combust. Flame 183 (2017) 271–282.

[3] A. Heinrich, S. Ganter, G. Kuenne, C. Jainski, A. Dreizler, J. Janicka, 3D numerical simulation of a laminar experimental SWQ burner with tabulated chemistry, Flow Turbul. Combust. 100 (2) (2018) 535–559.

[4] S. Ganter, A. Heinrich, T. Meier, G. Kuenne, C. Jainski, M. C. Rißmann, A. Dreizler, J. Janicka, Numerical analysis of laminar methane–air side-wall-quenching, Combust. Flame 186 (2017) 299–310.

[5] T. Häber, R. Suntz, Effect of different wall materials and thermal-barrier coatings on the flame-wall interaction of laminar premixed methane and propane flames, Int. J. Heat Fluid Flow 69 (2018) 95–105.

[6] C. Strassacker, V. Bykov, U. Maas, Redim reduced modeling of quenching at a cold wall including heterogeneous wall reactions, Int. J. Heat Fluid Flow 69 (2018) 185–193.

[7] D. Mejia, L. Selle, R. Bazile, T. Poinsot, Wall-temperature effects on flame response to acoustic Oscillations, Proc. Combust. Inst. 35 (3) (2015) 3201–3208.

[8] H. Kosaka, F. Zentgraf, A. Scholtissek, L. Bischoff, T. Häber, R. Suntz, B. Albert, C. Hasse, A. Dreizler, Wall heat fluxes and co formation/oxidation during laminar and turbulent side-wall quenching of methane and dme flames, Int. J. Heat Fluid Flow 70 (2018) 181–192.

[9] T. Poinsot, D. C. Haworth, G. Bruneaux, Direct simulation and modeling of flame-wall interaction for premixed turbulent combustion, Combust. Flame 95 (1-2) (1993) 118–132.

[10] M. Saffman, Parametric studies of a side wall quench layer, Combust. Flame 55(2) (1984) 141–159.

[11] P. Zhao, L. Wang, N. Chakraborty, Analysis of the flame-wall interaction in premixed turbulent combustion, J. Fluid Mech. 848 (2018) 193-218.

[12] M. Mann, C. Jainski, M. Euler, B. Böhm, A. Dreizler, Transient flame-wall interactions, experimental analysis using spectroscopic temperature and CO concentration measurements, Combust. Flame 161 (9) (2014) 2371–2386.

[13] Y. Luo, C. Strassacker, X. Wen, Z. Sun, U. Maas, C. Hasse, Strain Rate Effects on Head-on Quenching of Laminar Premixed Methane-air flame. Flow Turbul. Combust. 106 (2021) 631–647.

[14] A. Gruber, R. Sankaran, E. Hawkes, J. Chen, Turbulent flame–wall interaction: a direct numerical simulation study, J. Fluid Mech. 658 (2010) 5–32.

[15] P. Popp, M. Baum, Analysis of wall heat fluxes, reaction mechanisms, and unburnt hydrocarbons during the head-on quenching of a laminar methane flame, Combust. Flame 108 (3) (1997) 327–348.

[16] F. Zhang, T. Zirwes, T. Häber, H. Bockhorn, D. Trimis, R. Suntz, Near Wall Dynamics of Premixed Flames, Proc. Comubst. Inst. 38 (2) (2021) 1955-1964.

[17] T. Zirwes, T. Häber, F. Zhang, H. Kosaka, A. Dreizler, M. Steinhausen, C. Hasse, A. Stagni, D. Trimis, R. Suntz, H. Bockhorn, Numerical Study of Quenching Distances for Side-wall Quenching Using Detailed Diffusion and Chemistry, Flow Turbul. Combust. 106 (2021) 649-679.

[18] U. Ahmed, N. Chakraborty, M. Klein, Scalar Gradient and Strain Rate Statistics in Oblique Premixed Flame–Wall Interaction Within Turbulent Channel Flows, Flow Turbul. Combust. 106 (2021) 701–732.

[19] H. Wang, G. Chen, K. Luo, E.R. Hawkes, J.H. Chen, J. Fan, Turbulence/flame/wall interactions in non-premixed inclined slot-jet flames impinging at a wall using direct numerical simulation, Proc. Comubst. Inst. 38 (2) (2021) 2711-2720.

[20] H. Wang, Z. Wang, K. Luo, E.R. Hawkes, J.H. Chen, J. Fan, Direct numerical simulation of turbulent boundary layer premixed combustion under auto-ignitive conditions, Combust. Flame. 228 (2021) 292-301

[21] M. Steinhausen, T. Zirwes, F. Ferraro, S. Popp, F. Zhang, H., Bockhorn, C. Hasse, Turbulent flame-wall interaction of premixed flames using Quadrature-based Moment Methods (QbMM) and tabulated chemistry: an a priori analysis. Int. J. Heat Fluid Flow 93 108913 (2021).

[22] F. Zhang, H. Bonart, T. Zirwes, P. Habisreuther, H. Bockhorn, N. Zarzalis, Direct numerical simulation of chemically reacting flows with the public domain code OpenFOAM, in: High Performance Computing in Science and Engineering'14, Springer, 2015, p. 221.

[23] T. Zirwes, F. Zhang, J. A. Denev, P. Habisreuther, H. Bockhorn, Automated code generation for maximizing performance of detailed chemistry calculations in OpenFOAM, in: High Performance Computing in Science and Engineering'17, Springer, 2018, p. 189–204.

[24] T. Zirwes, F. Zhang, P. Habisreuther, M. Hansinger, H. Bockhorn, M. Pfitzner, D. Trimis, Quasi-DNS Dataset of a Piloted Flame with Inhomogeneous Inlet Conditions, Flow Turbul. Combust. 104 (2019) 997–1027.

[25] T. Zirwes, F. Zhang, J. A. Denev, P. Habisreuther, H. Bockhorn, D. Trimis, Improved Vectorization for efficient chemistry computations in OpenFOAM for large scale combustion simulations, in: High Performance Computing in Science and Engineering'18, Springer, 2019, p. 209.

[26] G. P. Smith, D. Golden, M. Frenklach, N. Moriarty, B. Eiteneer, M. Goldenberg, C. Bowman, R. Hanson, S. Song, W. Gardiner Jr, et al., Grimech 3.0 reaction mechanism, Sandia National Laboratory, 2000.

[27] J.E. Rivera, R.L. Gordon, M. Talei, Flame-wall interaction of a forced laminar premixed propane flame: Flame dynamics and exhaust CO emissions, Proc. Comubst. Inst. 37 (4) (2019) 5385-5392.

[28] R. Palulli, M. Talei, R.L. Gordon, Unsteady flame–wall interaction: Impact on CO emission and wall heat flux, Comubst. Flame 207 (2019) 406-416.

[29] F. Zhang, T. Zirwes, P. Habisreuther, H. Bockhorn, Effect of unsteady stretching on the flame local dynamics, Combust. Flame 175 (2017) 170-179.

[30] T. Zirwes, F. Zhang, Y. Wang, P. Habisreuther, J.A. Denev, Z. Chen, H. Bockhorn, D. Trimis, In-situ flame particle tracking based on barycentric coordinates for studying local flame dynamics in pulsating Bunsen flames, Proc. Combust. Inst. 38(2) (2021) 2057-2066.

[31] F. Zhang, T. Zirwes, Y. Wang, Z. Chen, H. Bockhorn, D. Trimis, D. Stapf, Dynamics of Premixed Hydrogen/Air Flames in Unsteady Flow. Phys. Fluids 34 (2022), 085121.